

Regulation of Murine Telomere Length by *Rtel*: An Essential Gene Encoding a Helicase-like Protein

Hao Ding,^{1,7} Mike Schertzer,^{2,7} Xiaoli Wu,¹
Marina Gertsenstein,¹ Sara Selig,^{2,4}
Makoto Kammori,² Reza Pourvali,² Steven Poon,²
Irma Vulto,² Elizabeth Chavez,² Patrick P.L. Tam,³
Andras Nagy,^{1,5} and Peter M. Lansdorp^{2,6,*}

¹Mount Sinai Hospital
Samuel Lunenfeld Research Institute
Toronto, Ontario, M5G 1X5

²Terry Fox Laboratory
British Columbia Cancer Agency
Vancouver, British Columbia, V5Z 1L3
Canada

³Embryology Unit
Children's Medical Research Institute
University of Sydney
Westmead, New South Wales, 2145
Australia

⁴Rambam Medical Center and
Technion Faculty of Medicine
Haifa 31096
Israel

⁵Department of Molecular and Medical Genetics
University of Toronto
Toronto, Ontario, M5S 1A8

⁶Department of Medicine
University of British Columbia
Vancouver, British Columbia, V5Z 4E3
Canada

Summary

Little is known about the genes that regulate telomere length diversity between mammalian species. A candidate gene locus was previously mapped to a region on distal mouse Chr 2q. Within this region, we identified a gene similar to the *dog-1* DNA helicase-like gene in *C. elegans*. We cloned this *Regulator of telomere length (Rtel)* gene and inactivated its expression in mice. *Rtel*^{-/-} mice died between days 10 and 11.5 of gestation with defects in the nervous system, heart, vasculature, and extraembryonic tissues. *Rtel*^{-/-} embryonic stem cells showed telomere loss and displayed many chromosome breaks and fusions upon differentiation in vitro. Crosses of *Rtel*^{+/-} mice with *Mus spretus* showed that *Rtel* from the *Mus musculus* parent is required for telomere elongation of *M. spretus* chromosomes in F1 cells. We conclude that *Rtel* is an essential gene that regulates telomere length and prevents genetic instability.

Introduction

Telomeres are DNA-protein complexes at the ends of linear eukaryotic chromosomes that play a critical role in maintaining chromosome stability (Zakian, 1995;

Blackburn, 2001). In most eukaryotic species, telomeric DNA consists of short G-rich repeat sequences synthesized by telomerase (Greider and Blackburn, 1985; Singer and Gottschling, 1994). In vertebrates, telomeric DNA consists of a double-strand region composed of TTAGGG repeats (Moyzis et al., 1988). The very end of chromosomes consists of a 3' single-strand G-rich overhang (Makarov et al., 1997; McElligott and Wellinger, 1997) that invades into the duplex telomeric repeat array to form a T loop structure (Griffith et al., 1999). An important function of telomeres is to distinguish normal chromosome ends from double-strand breaks, yet it is not clear exactly how the structure of telomere ends differs from sites of DNA damage (de Lange, 2002). Most likely activities that are specific for telomere maintenance (such as telomerase) are recruited to telomeres via proteins that bind directly or indirectly to telomere repeats (Blackburn, 2001; Vega et al., 2003). In the absence of such proteins, DNA repair-specific activities are recruited to chromosome ends that can trigger chromosome fusions (Mieczkowski et al., 2003) and end resection (Hackett and Greider, 2003) or induce other forms of potentially lethal DNA damage responses (Takai et al., 2003; Zhu et al., 2003).

Telomeric DNA is lost in cells because of incomplete replication of lagging strand DNA (Greider, 1996; McEachern et al., 2000), C strand degradation (Makarov et al., 1997), oxidative stress (von Zglinicki, 2002), and possibly other mechanisms. Telomerase is dispensable in cells with sufficiently long telomeres (Blasco et al., 1997), but cells with short telomeres that lack telomerase activity typically lose the ability to proliferate after a variable number of cell divisions (Blackburn, 2001). While the precise role of telomerase and telomeres in the proliferation of various cell types is subject to extensive investigations, it is clear that a minimum number of telomere repeats is required at each chromosome end for proper telomere function and to distinguish telomeres from double-strand breaks.

The average length of telomere repeats is set by an equilibrium between the mechanisms that lengthen and shorten telomere tracts. It is not known which factors are most important in establishing the average telomere length in cells or the mechanisms that generate telomere length diversity between species. In a previous study, the genetic regulation of telomere length was investigated by using two interfertile species of mice, which differ in their telomere length (Zhu et al., 1998). *Mus musculus* (telomere length >25 kb) and *Mus spretus* (telomere length 5–15 kb) were used to generate F1 crosses and reciprocal backcrosses, which were then analyzed for regulation of telomere length. This analysis indicated the presence of a dominant and transacting mechanism capable of extensive elongation of telomeres in somatic cells after fusion of parental germline cells with discrepant telomere lengths. A genome-wide screen of F1 backcrosses using *M. spretus* as the recurrent parent identified a 5 cM region on distal chromosome 2 that predominantly controls the observed spe-

*Correspondence: plansdor@bccrc.ca

⁷These authors contributed equally to this work.

cies-specific telomere length regulation (Zhu et al., 1998).

Among the candidate genes in this region, we identified the mouse homolog of the human novel helicase-like (NHL) gene (Bai et al., 2000). In order to study a possible role of this gene in telomere length regulation, we decided to first study one of the two most similar genes in *C. elegans*, the *dog-1* gene, for which a null mutant was readily available. While *dog-1* mutants displayed no clear telomere phenotype, they showed a highly unusual mutator phenotype characterized by deletions of G-rich DNA throughout genomic DNA (Cheung et al., 2002). Deletions in *dog-1* mutants invariably originated around the 3' end of the G tracts and typically were between 100 and 200 nucleotides in length. Such deletions were observed in ~50% of genomic polyguanine tracts above a threshold length of more than 18 consecutive Gs with a frequency that increased with the length of the tract. These results are consistent with a role for the DOG-1 protein in the resolution of higher order structures of G-rich DNA, such as guanine quadruplex DNA (Sen and Gilbert, 1988; Williamson et al., 1989), that could arise stochastically during lagging strand replication of G-rich template sequences (Cheung et al., 2002). In view of these findings in *C. elegans* and the well-known ability of telomeric G strands to assume G4 DNA structures in vitro (Sen and Gilbert, 1988; Williamson et al., 1989; Parkinson et al., 2002), we decided to study a possible role of the murine *Rtel* gene in telomere length regulation by disrupting its expression in vitro and in vivo.

Results

Genomic Organization of the *Rtel* Locus and Alternative Splicing of *Rtel* Transcripts

The murine *Rtel* gene has 34 exons, encompasses 36.6 kb of genomic DNA, and is located within 1 Mb of the telomere on chromosome 2q (Figures 1A and 1B). Northern blot analysis of transcripts yielded a species of ~4 kb in both *M. musculus* and *M. spretus*. No major differences between the two species were observed in ~1.5 kb of putative *Rtel* promoter sequences upstream of the first *Rtel* exon and *Rtel* transcript levels in different tissues varied in parallel (data not shown). Analysis of cDNA clones from *M. musculus*, *M. spretus*, and F1 cells showed several splice variants involving the last four exons of the *Rtel* gene (Figure 1C and dotted box in Figure 1A). Whereas full-length *M. musculus Rtel* transcripts were readily obtained, most (>90%) *M. spretus Rtel* transcripts were missing 18 or more bp at the C terminus (Figure 1C).

Rtel Encodes a Highly Conserved Protein with Characteristic Helicase Motifs

Full-length *Rtel* transcripts are predicted to encode a 1209 amino acids (aa) protein in *M. musculus* and *M. spretus* (see Supplemental Figure S1 at <http://www.cell.com/cgi/content/full/117/7/873/DC1>). Both proteins are highly homologous (>98% aa identity) to each other and 74% identical to the human NHL protein (Bai et al., 2000). The sequence identity is even higher for the first 750 aa containing the seven domains of known helicases (Fig-

ure 1D). Of note, both RTEL and NHL contain a conserved eight-amino acid PIP-box motif near the carboxy terminus that is commonly found in proteins capable of interacting with proliferating cell nuclear antigen (PCNA) (Warbrick, 2000). The protein encoded by the most common splice variant in *M. spretus* (AY481613) is lacking six amino acids (AHFSKP) that are also absent in the human NHL protein. As a result, this splice variant contains a predicted CK1 phosphorylation site (Kreegipuu et al., 1999) that is not present in the full-length protein.

Expression of *Rtel* in Tissues and Cells

Rtel expression was analyzed in mouse embryos and adult tissues to reveal its potential function. Details of this analysis are shown in Figure 2 and Supplemental Figure S2 (on the *Cell* web site). *Rtel* was widely expressed in E8.5 and E9.5 embryos and showed a more restricted expression pattern at E13.5–E15.5. In general, *Rtel* expression in embryos appeared to coincide with areas of actively proliferating cells (see Supplemental Figure S2). In adult mice, *Rtel* expression was detectable by Northern hybridization in spleen, thymus, Peyer's patches, kidney, and intestine but not in brain, heart, lung, skeletal muscles, skin, and white fat tissue (Figure 2A). In the adult gonad, *Rtel* was expressed highly in the testis, mainly in the spermatogonia and meiotic spermatocytes (Figure 2B). *Rtel* expression was studied in relation to cell proliferation in adult tissues in three experimental models. Significant induction of *Rtel* expression was observed in actively regenerating muscle and liver as well as in mitogen-stimulated spleen cells (see Supplemental Figure S2).

To examine the subcellular localization of RTEL, mouse embryonic stem cells were transiently transfected with a plasmid encoding V5 epitope-tagged RTEL. Cells expressing the transgene (<1% of total) were easily recognized by bright nuclear staining, which, in all cells, had a fine granular appearance that did not include nucleoli or areas of heterochromatin (Figures 2C and 2D). In view of the expression of RTEL in proliferating cells and tissues and the presence of a predicted PCNA binding site in RTEL (Figure 1D), the expression of RTEL relative to PCNA was also examined (Figures 2D–2H). PCNA was expressed at variable levels in most ES cells (Figure 2D). While, in cells that expressed both PCNA and the transgene, the nuclear staining pattern appeared very similar, only a minority of the small nuclear foci appeared to directly overlap (Figure 2H). Staining of replication foci using anti-BrdU yielded similar results, and epitope-tagged RTEL did not significantly colocalize with either telomeric DNA or antibodies specific for telomere binding proteins (data not shown).

Taken together, these data indicate that *Rtel* expression is widespread in dividing cells during embryonic development, in adult cells that are induced to proliferate, and, constitutively, in some adult tissues, most notably the testis. RTEL expression in ES cells appears restricted to the nucleus in numerous foci that appear similar but overlap only partially with replication foci containing PCNA.

Generation of a Null Mutation of *Rtel*

To further study *Rtel* function, the *Rtel* locus was mutated in ES cells by homologous recombination. A tar-

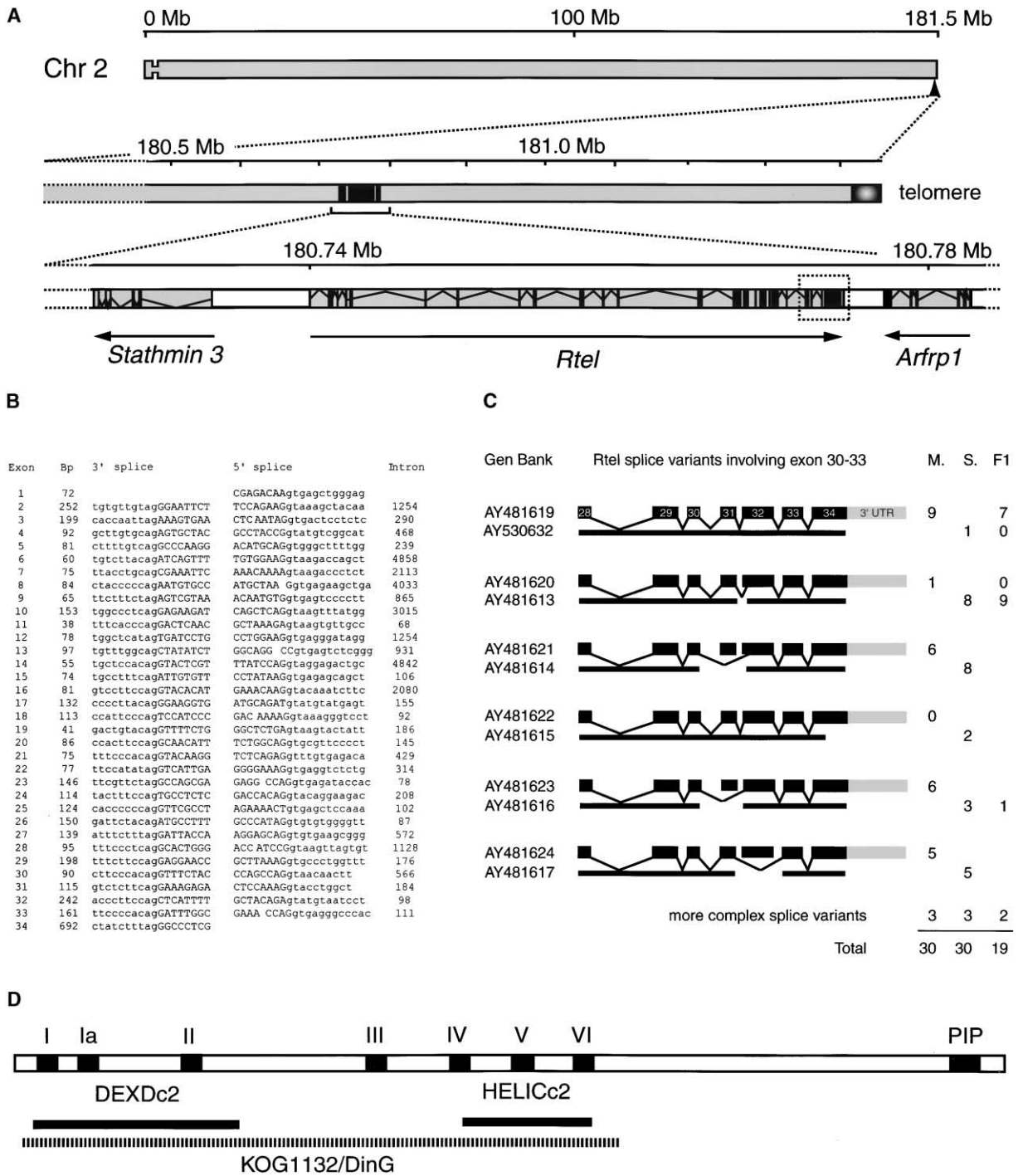


Figure 1. Gene Structure, Splice Junction Sites, and Splice Variants of the *Rtel* Gene and Conserved Functional Domains in the RTEL Protein
(A) Location of the *Rtel* within 1 Mb of the telomere at chromosome 2q. The *Rtel* gene encompasses 36.6 kb of genomic DNA and is flanked by the *Stathmin3* and *Arfrp1* genes. Alternative splicing involves the boxed area at the 3' end of the gene.
(B) Splice junction sites and exon size of the *M. musculus Rtel* gene. Exon sequences are in capitalized letters. Intron sequences are in lowercase.
(C) *Rtel* splice variants obtained from cDNAs derived from *M. musculus* and *M. spretus* testes and *(M. musculus × M. spretus)* F1 spleen cells. Regions homologous to the coding sequence of cDNA are indicated by black boxes, and the 3' UTR is indicated as a gray box. Skipping of a full or partial exon is indicated by brackets below the exons. The predicted protein products are shown as black bars under each splice variant. The number of times a given splice variant sequence was observed is shown.
(D) Conserved functional domains in the predicted RTEL amino acid sequence include the seven characteristic helicase motifs indicated by roman numbers. RTEL is classified in the NCBI conserved domain database as a member of the KOG1132, helicase of the DEAD superfamily (replication, recombination, and repair), and as a member of the DinG, Rad3-related DNA helicases containing both a DEXDc2 and a HELICc2 domain (Marchler-Bauer et al., 2003). A PIP box (encoded by exon 34) is present near the C terminus of the protein.

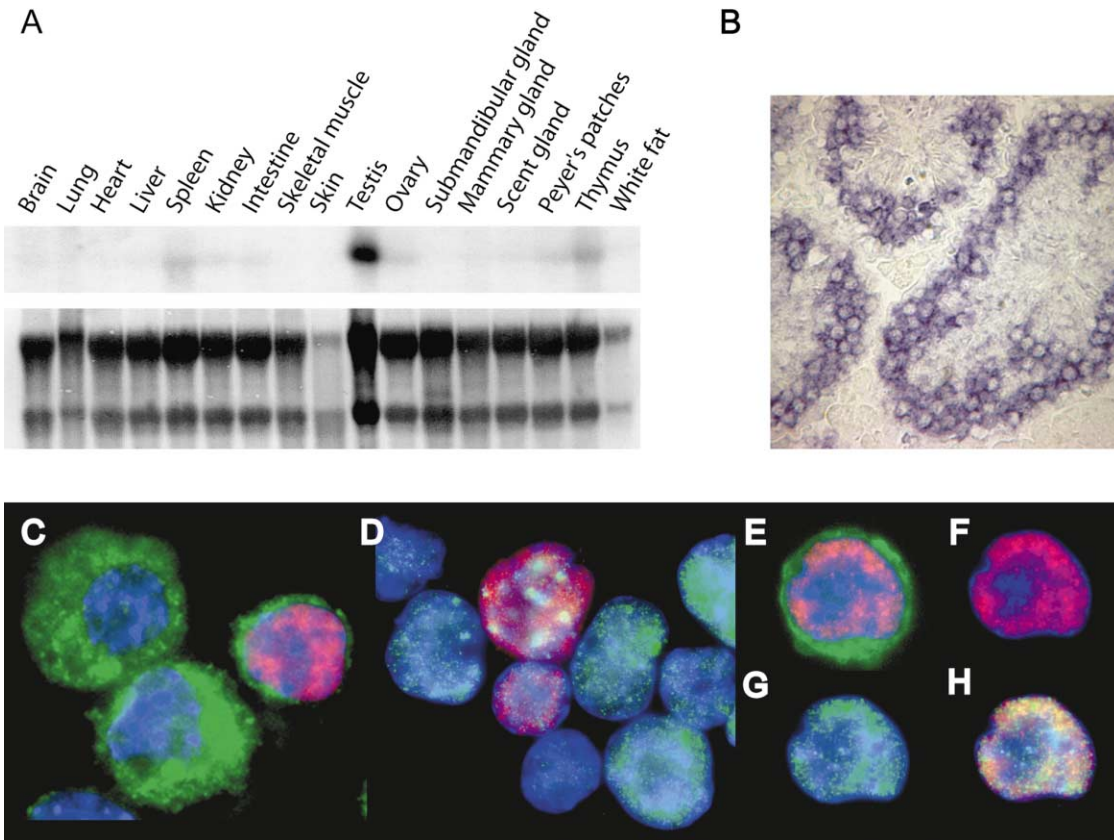


Figure 2. Rtel Expression in Adult Tissues

(A) Northern blot analysis of *Rtel* expression in the indicated adult mouse tissues. Lower panel shows the control blot analysis of total ribosomal RNAs for normalization.

(B) *Rtel* expression in adult testis revealed by in situ hybridization.

(C) Nuclear localization of V5 epitope-tagged RTEL. Murine embryonic stem cells transfected with V5 epitope-tagged RTEL were stained with mouse monoclonal anti-V5 (shown in red), BODIPY 650/665 phalloidin to label actin (labeled green, mainly present in the cytoplasm), and DAPI (shown in blue) to stain DNA. Note the fine granular nuclear staining of a single cell expressing V5-RTEL, which appears excluded from a large area staining weakly with DAPI (presumably the nucleolus) and several heterochromatic areas staining brightly with DAPI.

(D–H) Similar nuclear staining of RTEL and PCNA. ES cells transfected with V5-tagged RTEL (red fluorescence) were counterstained with rabbit anti-PCNA, goat anti-rabbit FITC (green fluorescence), and DAPI. Note the variable nuclear expression of PCNA in cells and the partial overlap of RTEL and PCNA fluorescence. The latter is more clearly shown in (F)–(H), showing individual staining for RTEL (F) and PCNA (G) as well as the overlap in fluorescence (H).

getting vector with a splice acceptor (SA)-*IRES*- β geo-*pA* cassette was used to replace exons 7–9, which encode residues 180–255, comprising the second DNA helicase domain, in order to disrupt *Rtel* transcription 3' to the start of exon 7 (Figure 3A). Correct homologous recombination in R1 ES cells was confirmed by Southern blot analysis (Figures 3B and 3C). Two independent ES clones were used to produce germline-transmitting chimeras that were bred with 129S1 females to produce mutant mice.

LacZ transgene expression in *Rtel*^{+/-} embryos (data not shown) corresponded accurately to the expression pattern established by in situ hybridization (Supplemental Figure S2). *Rtel* mRNA was absent by Northern blot hybridization in homozygous mutants (Figure 3E) and in *Rtel*^{-/-} ES cells derived from *Rtel* homozygous blastocysts (Figure 3F), indicating that the targeted mutation gave rise to a null allele.

Embryonic Lethality of *Rtel*^{-/-} Homozygotes

Homozygous null mutant embryos were present at the expected Mendelian frequency at E8.5–E10.5 (data not

shown). They were absent from E11.5 onward and among the newborn of intercrosses of heterozygous 129S1 or outbred mutant mice (data not shown), indicating that loss of *Rtel* function leads to embryonic lethality. *Rtel*^{-/-} embryos at E8.5–E10.5 showed progressive abnormalities in various tissues, particularly in rapidly proliferating tissues such as the nervous system, the heart, the vasculature, and extraembryonic tissues. Subcutaneous hematomas were found at various sites in the body and limbs at E10.5 and could underpin the embryonic lethality. A detailed characterization of the growth abnormalities in *Rtel*^{-/-} embryo is provided in Supplemental Data.

Defective Differentiation and Telomere Dysfunction in *Rtel*^{-/-} ES Cells

To further study the role of *Rtel* in ES cells, we derived several *Rtel*^{-/-} and *Rtel*^{+/+} ES lines from *Rtel*^{+/-} (129S1 background) intercrosses. Relative to *Rtel*^{+/+} cells, *Rtel*^{-/-} ES cells were more difficult to recover from frozen stock. However, once established, no major differ-

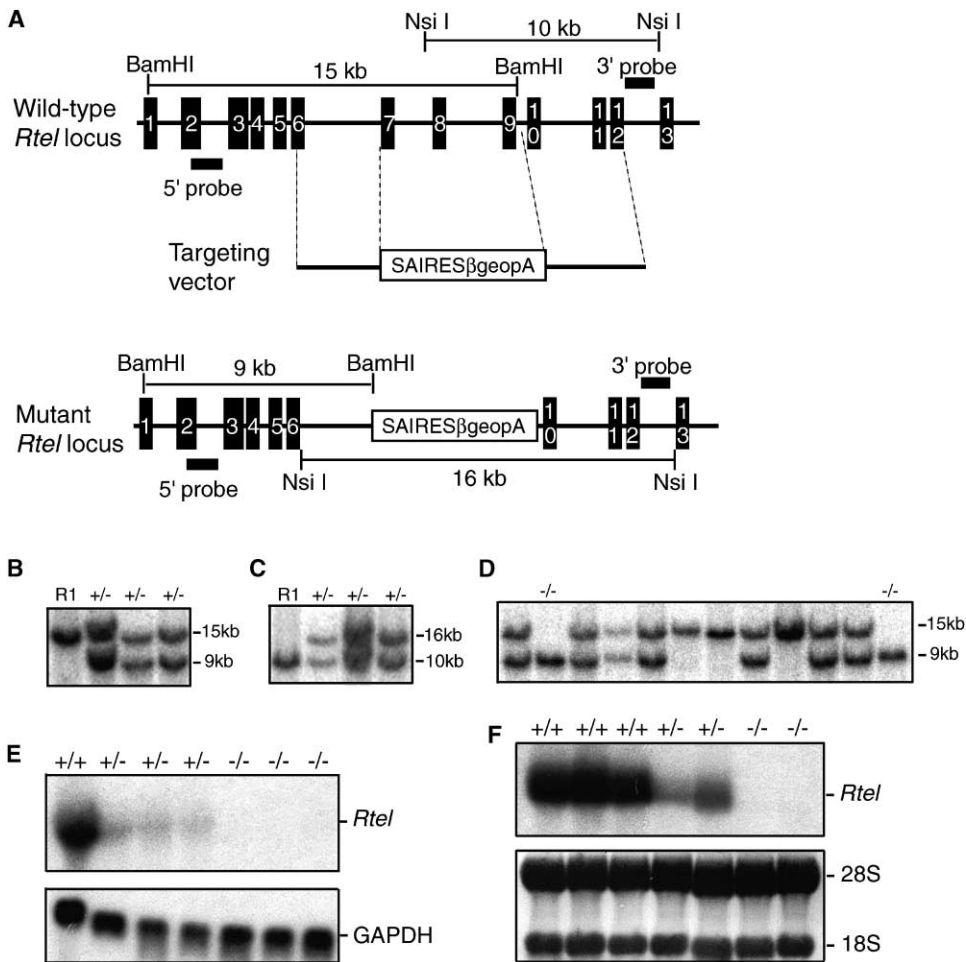


Figure 3. Targeted Disruption of *Rtel* by Homologous Recombination

(A) Schematic representation of exons 1–13 of the mouse *Rtel* locus, the targeting vector, and the mutant allele. Black boxes represent exons according to sequence comparison of *Rtel* cDNA and corresponding genomic sequences. Exons 7–9 were deleted and replaced with a splicing acceptor (SA)-linked IRES β geo cassette to generate a null allele. The locations of the hybridization probes (5' probe and 3' probe) for Southern blot analysis are shown.

(B) Southern blot analysis of ES clones with insertion of targeting vector. The genomic DNA was digested with *Bam*HI and probed with 5' probe. The wild-type allele produced a 15.0 kb fragment, and the targeted allele produced a 9.0 kb fragment. The genomic DNA of wild-type R1 ES cells was used as a control.

(C) Southern blot analysis of targeted ES clones using the 3' probe. The genomic DNA was digested with *Nsi*I and hybridized with the 3' probe, giving a wild-type allele of 10.0 kb and a mutant allele of 16.0 kb.

(D) Southern blot analysis of ES cells derived from blastocysts of *Rtel*^{+/-} (129Sv background) intercrosses. Genomic DNA was digested with *Bam*HI and probed with the 5' probe. Two homozygous ES clones produced only a mutant allele of 9.0 kb.

(E) Northern blot analysis of *Rtel* mRNA in the E9.5 embryos of the indicated genotypes. A 750 bp cDNA fragment covering the 3' end of *Rtel* coding sequence was used as a probe. GAPDH cDNA hybridization was used as a normalization control.

(F) Northern blot analysis of total RNA isolated from the ES cells shown in (D). The 28S and 18S ribosomal RNAs are shown as normalization controls.

ences in the growth rate of *Rtel*^{+/+} and *Rtel*^{-/-} ES cells were recorded. In contrast, when cells were cultured in medium without leukemia inhibitory factor (LIF) to induce their differentiation, striking differences in the frequency and size of day 5 embryoid bodies between *Rtel*^{+/+} and *Rtel*^{-/-} ES cells were observed (Figure 4A). Whereas *Rtel*^{+/+} and *Rtel*^{+/-} ES cells yielded 367 \pm 101 and 274 \pm 83 embryoid bodies per 1500 cells plated, this number was 66 \pm 19 for *Rtel*^{-/-} ES cells. To study the nature of the defect in differentiating *Rtel*^{-/-} ES cells, the cell cycle distribution of ES cells grown without LIF was analyzed using 5-bromo-2'-deoxyuridine (BrdU) incorporation. In *Rtel*^{+/+} ES cells, the fraction of cells in

S phase decreased upon differentiation (Figure 4B), consistent with previous observations (Aladjem et al., 1998). In contrast, a large number of cell fragments (reflecting cell death) and an almost complete loss of BrdU-labeled cells was observed in *Rtel*^{-/-} cells cultured without LIF for 3 days (Figure 4B, bottom panels).

To study a possible role of RTEL in telomere homeostasis, the average telomere length as well as the telomere length of individual chromosome ends in *Rtel*^{+/+}, *Rtel*^{+/-}, and *Rtel*^{-/-} ES cells was studied using flow FISH (Figure 4C), terminal restriction fragment length by Southern blot analysis (Figure 4D), and Q-FISH (Figures 4E–4G), respectively. Flow FISH analysis showed that

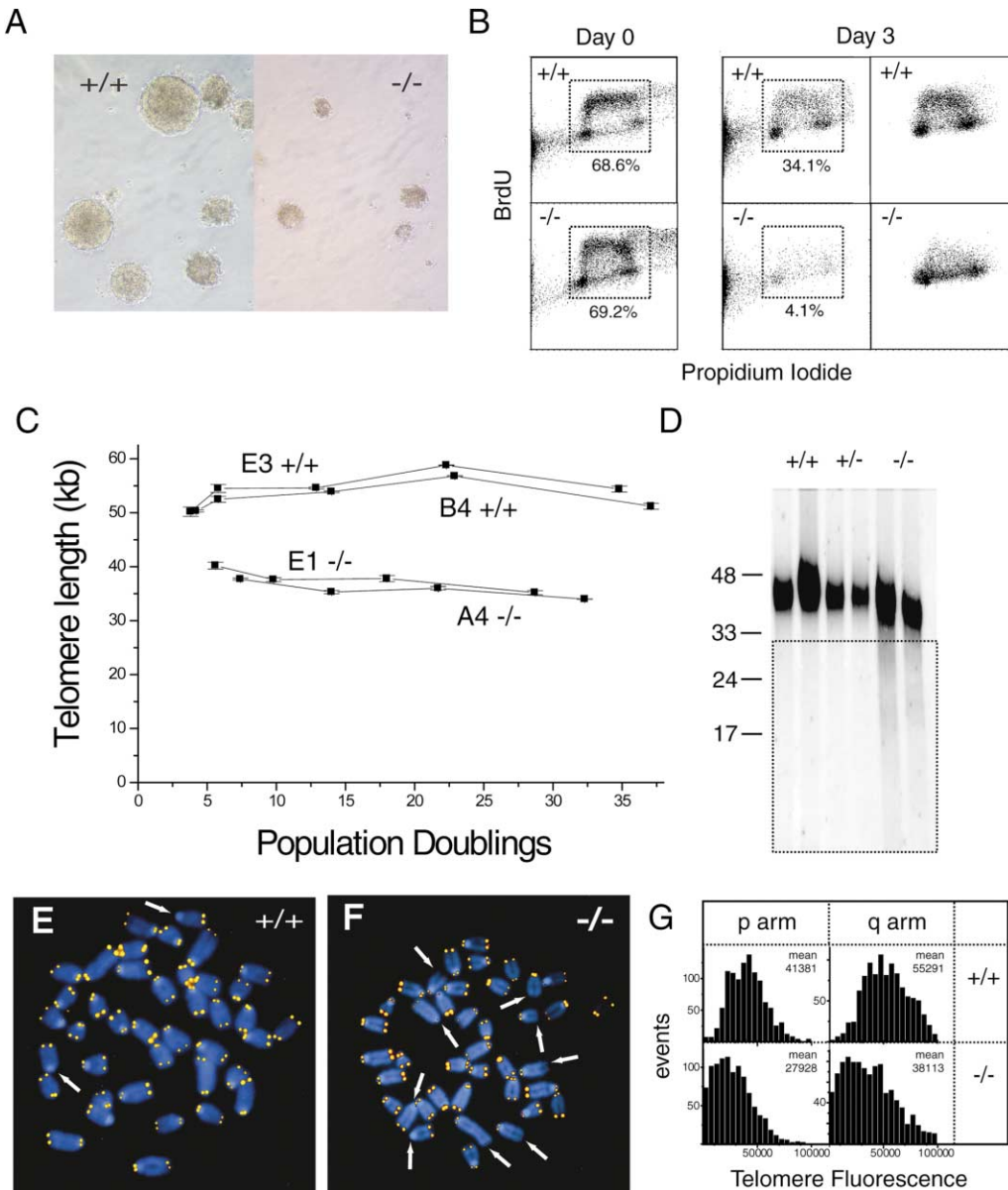


Figure 4. Defective Differentiation and Telomere Phenotype of *Rtel*^{-/-} ES Cells

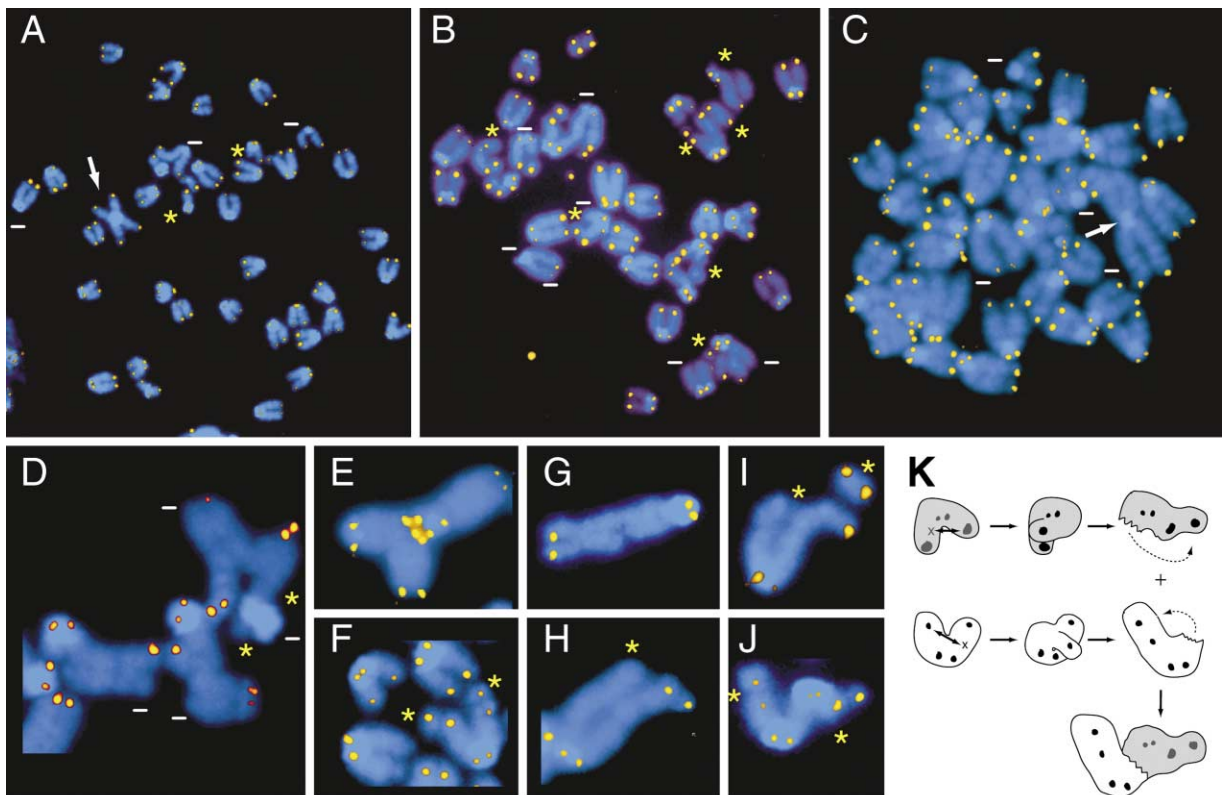
(A) Differentiation of *Rtel*^{+/+} and *Rtel*^{-/-} ES cells cultured for 20 population doublings in liquid culture prior to differentiation in the absence of LIF in methylcellulose. Note that colonies observed at day 5 are notably smaller in *Rtel*^{-/-} cells.

(B) Cell cycle distribution of *Rtel*^{+/+} and *Rtel*^{-/-} ES cells before and after induction of differentiation by removal of LIF from the culture medium. Cells were pulsed with BrdU for 30 min prior to harvest to distinguish cells in the G1, S, and G2M phase of the cell cycle. Prior to differentiation the majority of intact *Rtel*^{+/+} and *Rtel*^{-/-} cells (boxed areas, left quadrants) are in S phase (cells with high BrdU content that connect G1 cells with low BrdU and low PI fluorescence to G2M cells with low BrdU and high DNA content). After 3 days of culture without LIF, very few (4.1%) intact cells are recovered from cultures of *Rtel*^{-/-} ES cells (middle quadrants), and such cells contain very few cells in S phase (right quadrant, events within boxed area of middle quadrant only). In contrast, many cells in S phase (34.1%) were recovered from *Rtel*^{+/+} control cultures. The percentage of events in the boxed area relative to the total number of acquired events is shown.

(C) Telomere length (mean and standard deviation from duplicate measurements) in undifferentiated *Rtel*^{+/+} (B4 and E3) and *Rtel*^{-/-} (A4 and E1) ES cells measured by flow FISH. Telomere length in *Rtel*^{-/-} cells is maintained at ~37 kb or around 68% of the length in *Rtel*^{+/+} cells (~54kb) over >25 population doublings.

(D) Telomere length in *Rtel*^{+/+}, *Rtel*^{+/-}, and *Rtel*^{-/-} ES cells measured by terminal restriction fragment (TRF) Southern blot analysis. Note that fragments with an estimated length of <30 kb (boxed area) are observed in *Rtel*^{-/-} cells but not *Rtel*^{+/+} and *Rtel*^{+/-} cells.

(E-G) Telomere length analysis in *Rtel*^{+/+} and *Rtel*^{-/-} ES cells using Q-FISH. Ends with low or undetectable telomere signals (arrows) are present in both *Rtel*^{+/+} (E) and *Rtel*^{-/-} ES cells (F) but are much more abundant in *Rtel*^{-/-} cells. (G) Q-FISH telomere length analysis in *Rtel*^{+/+} (E3) and *Rtel*^{-/-} (A4) undifferentiated ES cells at PD20. Quantitative analysis of >30 metaphase cells using images similar to those shown in (E) and (F). The mean fluorescence intensity (in arbitrary units) is indicated in the fluorescence histogram. Note the skewed distribution of telomeres and the large number of events with no or very little telomere signal in *Rtel*^{-/-} relative to *Rtel*^{+/+} cells.



L

	ES cell	Hours of differentiation												
		<i>Rtel</i> genotype	0			4			8			48		
			n	f	o	n	f	o	n	f	o	n	f	o
B4	+/+	1178	0	0	1180	1	0	1159	1	0	1687	2	1	
C1	+/+	1175	0	0	1168	0	0	1170	0	1				
E3	+/+										1643	4	1	
A4	-/-										1627	64	3	
E1	-/-	1197	0	0	1167	5	29	1085	7	32				
F2	-/-	1191	1	1	1118	4	10	1129	0	21	1915	34	5	

Figure 5. Chromosomal Abnormalities in Differentiating *Rtel*^{-/-} ES Cells

(A–J) Metaphase chromosomes (counterstained with DAPI, shown in blue) hybridized with fluorescently labeled PNA (shown in yellow) from *Rtel*^{-/-} ES cells grown for 4 or 8 hr without LIF to induce their differentiation. 4 hr, (A) and (D)–(J); 8 hr, (B) and (C). Note end-to-end fusions without detectable telomeric DNA at the junction site (arrows), chromosome ends with no detectable telomeric DNA (white bars), chromosome breaks and fragments (asterisks), and various other striking abnormalities (D–J).

(K) Possible sequence of events that gave rise to the abnormality shown in (J). Two independent chromosomes (white and gray, respectively) with widely different q arm telomere lengths occur lesions such as unresolved (T₂AG₃)_n G4 DNA (indicated by an X) at internal sites in one of the chromatids. Aberrant recombination between DNA at the internal site and telomeric DNA present at the sister chromatid results in a broken chromatid and displacement of the terminal fragment to the opposing chromatid. Fusion of the two broken ends on the two separate chromosomes could give rise to the abnormality seen in (J).

(L) Table indicating the number of chromosome fusions (f) in differentiating *Rtel*^{+/+} and *Rtel*^{-/-} ES cells. Other abnormalities (o) include chromosome and chromatid breaks and gaps, chromosome fragments, and tri- and multiradial formations. Chromosome fusions (f) are defined as juxtaposed chromosomes without detectable telomeric DNA at the junction site. n, the number of chromosomes that was analyzed. In total, 30 metaphase cells (4 and 8 hr) and 40 metaphase cells (48 hr) were analyzed, respectively. Nine out of 40 metaphase cells from F2 *Rtel*^{-/-} ES at 48 hr contained more than 60 chromosomes (aneuploidy). One E1 *Rtel*^{-/-} metaphase cell (4 hr) contained 13 of the 29 reported abnormalities, and ten out of 32 reported other abnormalities at 8 hr were also observed in a single E1 cell.

the average telomere length in *Rtel*^{+/+} and *Rtel*^{+/-} ES cells was kept relatively constant over 30 population doublings (PD) at a similar length of 53.7 ± 2.8 kb (Figure 4C) and 51.6 ± 0.7 kb (data not shown). In contrast, the telomere length in two separate *Rtel*^{-/-} ES cells was maintained at 36.7 ± 1.9 kb or ~68% of wild-type length over 30 PD (Figure 4C). Southern blot analysis and Q-FISH analysis revealed that this difference in average telomere length resulted from the presence of variably shortened telomeres in *Rtel*^{-/-} cells (boxed area in Figure 4D and skewed telomere length distribution in Figure 4G) next to telomeres of apparent wild-type length. Q-FISH analysis showed that, whereas occasional ends with a very faint or undetectable FISH signals were observed in *Rtel*^{+/+} ES cells (Figure 4E, arrows), such events were relatively abundant in *Rtel*^{-/-} ES cells (Figure 4F, arrows, and Figure 4G).

Taken together, the data indicate that lack of RTEL results in variable loss of telomere repeats in undifferentiated ES cells and maintenance of overall telomere length at around 68% of that observed in wild-type ES cells.

Cytogenetic Abnormalities in Differentiating *Rtel*^{-/-} ES Cells

To study chromosome abnormalities observed in differentiating *Rtel*^{-/-} ES cells in relation to telomeric DNA, Q-FISH telomere analysis was performed on chromosome spreads obtained from both *Rtel*^{+/+} and *Rtel*^{-/-} ES cells at various time intervals following induction of differentiation. Strikingly, a variety of chromosomal abnormalities was already observed in a minority of cells 4 hr following removal of LIF (Figure 5). Apart from end-to-end fusions (arrows) and ends without detectable telomere signal (bars), the chromosomal abnormalities that were observed included clusters of chromosomes joined at sites containing telomeric DNA (Figure 5E), various types of broken chromosomes and chromosome fragments (asterisks in Figures 5A, 5B, 5D, 5F, and 5H-5J), and chromatid gaps (Figure 5G). At later time points, the most abundant cytogenetic abnormalities were end-to-end fusions characterized by a lack of detectable telomere repeats at the junction site (Figure 5L).

The chromosomal abnormalities in differentiating *Rtel*^{-/-} ES cells indicate that RTEL is required to maintain the integrity of genomic as well as telomeric DNA. In order to explore possible similarities in genetic instability between *Rtel*^{-/-} cells and *dog-1* mutants (Cheung et al., 2002), we studied the stability of several G-rich sequences in genomic DNA from *Rtel*^{+/+} and *Rtel*^{-/-} ES cells (see Supplemental Data for details). No deletions or insertions were observed in seven genomic polyguanine tracts (G > 18), 14 genomic (TTAGGG)_n repeats (n > 6) and 11 genomic (CCCTG)_n repeats (n > 6).

Rtel Is Required to Elongate *M. spretus* Telomeres in Crosses with *M. musculus*

In a previous study, a trait involved in murine telomere length regulation was mapped to the Tlq1 locus on distal chromosome 2 (Zhu et al., 1998). In order to test the hypothesis that *Rtel* is the gene responsible for this trait, we first measured the average telomere length in spleen

cells from F1 littermates obtained from crosses between a *Rtel*^{+/-} 129SI inbred female and a *M. spretus* male using flow FISH. The results (shown in Figure 6A) confirmed that the average telomere length was long (43.3 kb) and short (9.3 kb) in the 129SI *M. musculus* and *M. spretus* parental cells, respectively. In the offspring, the average telomere length in cells from animals derived from two litters that inherited the wild-type *M. musculus* *Rtel* allele (n = 5) was significantly longer than in littermates (n = 7) that inherited the *Rtel* null allele from the *M. musculus* parent (Figure 6B). These results were confirmed by performing Q-FISH telomere length analysis of cells from F1 animals (Figures 6C and 6D). The telomere length in *M. spretus*-derived chromosomes in cells from F1 littermates with the *Rtel* null allele from the *M. musculus* parent (n = 5) was similar to that observed in parental *M. spretus* cells and was markedly shorter than in cells from littermates that inherited the wild-type *Rtel* allele from the *M. musculus* parent (n = 5, Figure 6D). This was true for three different cell types from all animals of three different litters. These results demonstrate that elongation of the shorter set of telomeres in chromosomes derived from the *M. spretus* parent in F1 cells requires *Rtel* expression from the *M. musculus* parent.

Discussion

In this study, we describe the organization, expression pattern, alternative splicing, and putative function of *Rtel*, a murine gene encoding a DNA helicase-like protein. *Rtel* is an essential gene in that lack of *Rtel* results in genomic instability and embryonic lethality. *Rtel*^{-/-} ES cells were found to grow relatively normal, be it with shortened telomeres, but showed genetic instability and defective growth upon differentiation in vitro. Crosses between *Rtel*^{+/-} mice and *M. spretus* revealed that *Rtel* from the *M. musculus* parent is required for elongation of telomeres in *M. spretus*-derived chromosomes. We conclude that *Rtel* is a dominant regulator of murine telomere length.

Rtel Mode of Action

The loss of telomere repeats and genetic instability in *Rtel*^{-/-} cells could result directly or indirectly from the absence of RTEL. Further studies on the biochemical properties and molecules interacting with RTEL are needed to delineate its precise function. However, based on the observations described in this paper and the sequence similarity between RTEL and the DOG-1 protein in *C. elegans* (Cheung et al., 2002), we speculate that the functions of RTEL and DOG-1 are comparable. According to this model, RTEL is required to resolve higher order structures of G-rich DNA such as G4 DNA that could arise during replication, transcription, DNA repair, and recombination of suitable G-rich DNA sequences (Figure 7). In the absence of RTEL, higher order structures of G-rich DNA at telomeres or elsewhere in the genome could trigger repair by homologous recombination. In general, repeat sequences pose a problem for repair by homologous recombination (Petes and Hill, 1988). For telomere repeats, the chances of a successful outcome could be further compromised by involvement

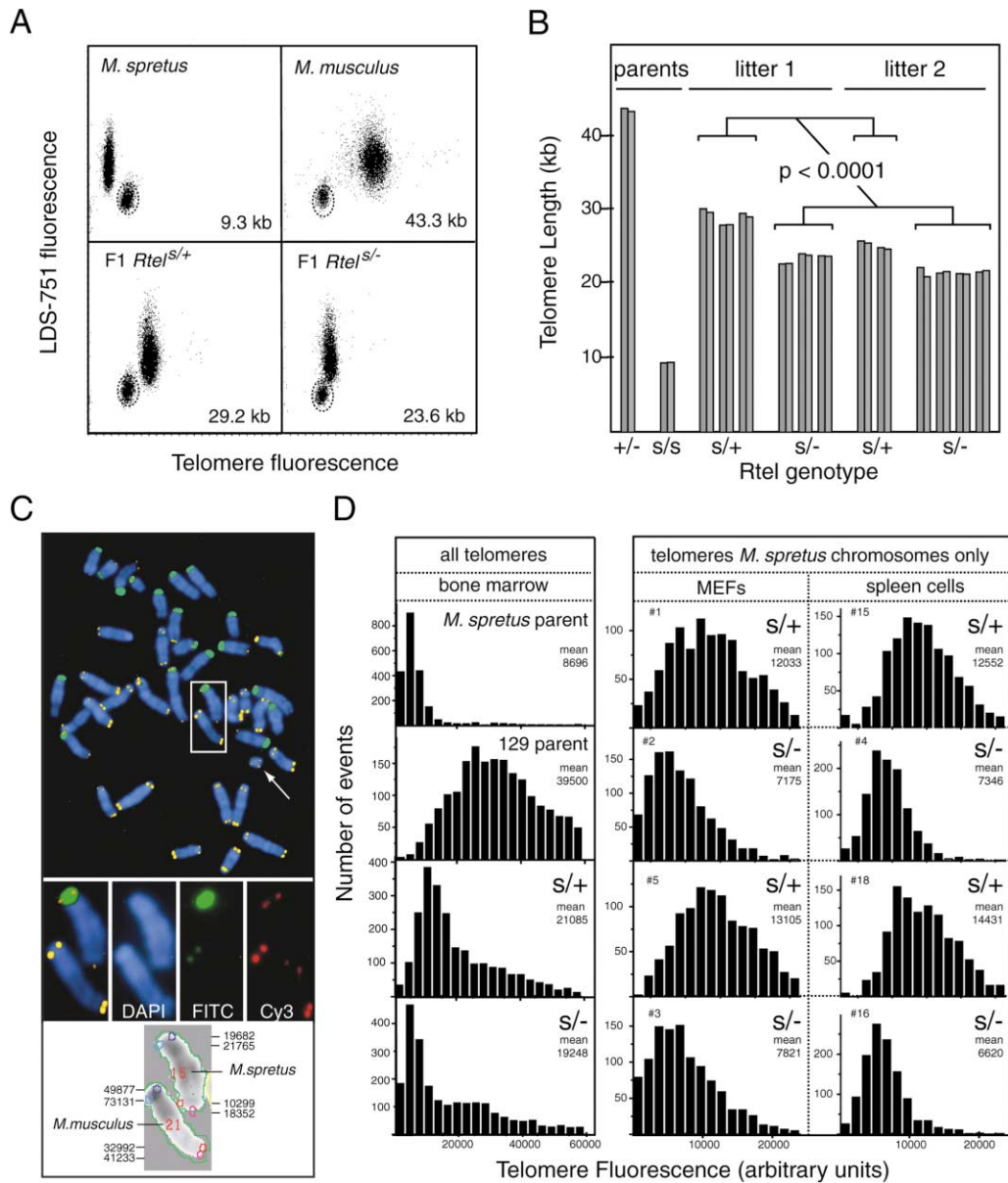


Figure 6. *M. musculus Rtel* Is Required for Elongation of *M. spretus* Telomeres in F1 Cells

(A and B) Flow FISH analysis. (A) Dot plot histogram of telomere versus LDS-751 fluorescence of spleen cells obtained from parents (top panels) and two representative F1 offspring (bottom panels) of a cross between a *M. spretus* male and a *Rtel*^{+/-} *M. musculus* (129) female. The dotted line represents the analysis gate for the fixed bovine thymocytes that were added to every sample as an internal reference for telomere length calculations (Baerlocher and Lansdorp, 2003).

(B) Telomere length in spleen cells from littermates derived from crosses between a *M. spretus* male and a *Rtel*^{+/-} *M. musculus* (129) female. Results of duplicate telomere length measurements by flow FISH of individual animals are shown. The difference in telomere length between F1 cells with (n = 5) and without the *M. musculus Rtel* gene (n = 7) is highly significant (p < 0.0001) using a hierarchical model (allowing for the nesting within litters).

(C and D) Analysis of telomere length at individual chromosome ends using Q-FISH. (C) Example of a multicolor FISH images used for Q-FISH analysis. Metaphase chromosomes in an embryonic fibroblast from the F1 offspring of a cross between a *M. spretus* male and a *Rtel*^{+/-} *M. musculus* (129) female. Cell were hybridized with a mixture of PNA probes for telomere repeats (probe labeled with Cy3, shown in yellow/red) and minor satellite repeats (labeled with FITC, shown in green). Note that the chromosomes derived from the *M. spretus* parent can be easily recognized by the much brighter staining, with the probe for repetitive sequences present at mouse centromeres (except the Y chromosome, arrow). The boxed area in the top panel is magnified in the lower panels which show individual (pseudo) colors and an example of the results of Q-FISH telomere length analysis generated using the TFL-Telo software program (Zijlmans et al., 1997).

(D) Quantitative analysis of telomere length in chromosomes from different cell types derived from the offspring of crosses between *Rtel*^{+/-} *M. musculus* (129) and *M. spretus* parents. The mean fluorescence intensity (in arbitrary units) for each cell type is shown in the fluorescence histogram. The telomere fluorescence in chromosomes derived only from the *M. spretus* parent (identified by bright green fluorescence as shown in Figure 6C) are shown in the panels on the right. Note that *M. spretus* telomeres are longer in F1 cells from animals that inherited the wild-type *M. musculus Rtel* allele than in F1 cells from animals that inherited the *M. musculus Rtel* null allele.

Wild type

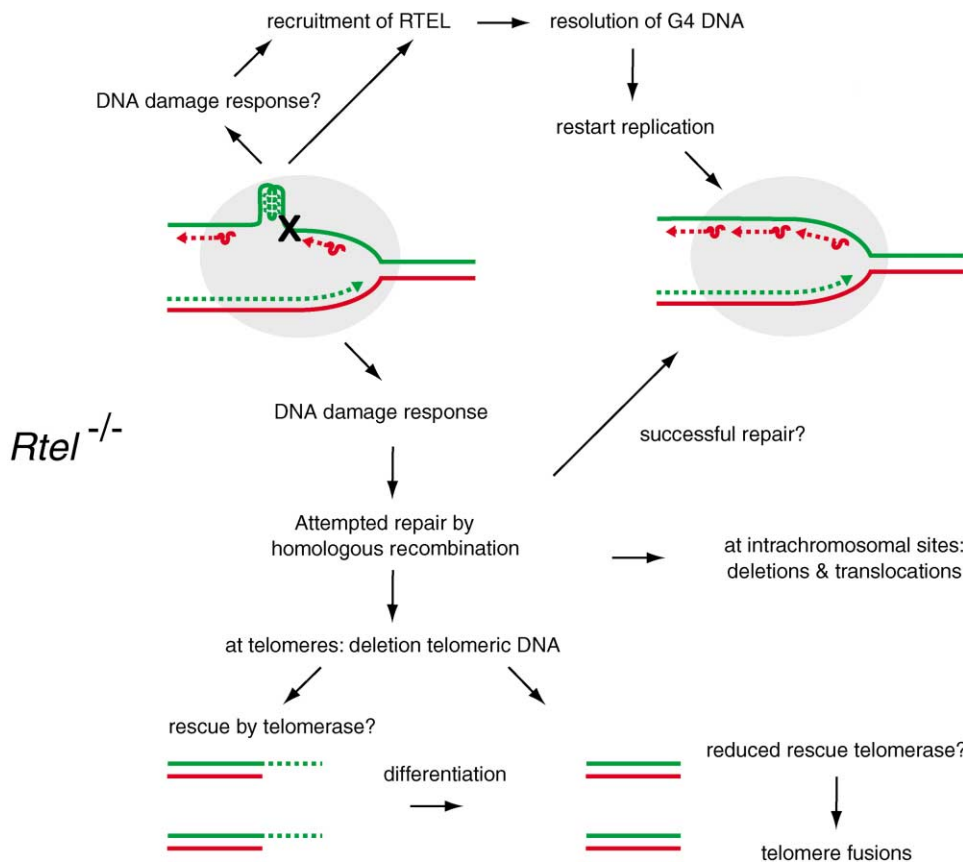


Figure 7. Model of RTEL Action

In both wild-type and *Rtel*^{-/-} cells, higher order structures of G-rich DNA such as guanine quadruplex (G4) DNA are postulated to arise sporadically and stochastically during lagging strand replication, repair, or recombination of suitable G-rich DNA sequences. (T₂AG₃)_n DNA is predicted to be particularly at risk for G4 DNA formation with the chance being proportional to the length of the repeat array. In wild-type cells, RTEL could be recruited to the G4 lesion either directly or via a DNA damage response and participate in its resolution. Effective interactions between G4 lesions and RTEL may depend on RTEL levels and could vary between RTEL isoforms. In the absence of RTEL, the G4 lesion could trigger DNA “repair” by homologous recombination. Involvement of the 3' chromosome ends in the initial lesion or the subsequent recombination reactions could result in deletions at telomeric sites (Figures 4C–4G) and more diverse abnormalities at intrachromosomal sites (Figure 5).

of the single-strand overhang (Makarov et al., 1997, McElligott and Wellinger, 1997) in the recombination reaction (Lustig, 2003; Zhu et al., 2003).

The above model is consistent with several of the observations reported here. First, the telomere length in *Rtel*^{-/-} ES shows an unusual distribution compatible with the presence of wild-type as well as variably shortened telomeres (Figures 4D and G). G4 DNA at telomeres could presumably form anywhere along a telomere tract, resulting in deletions of variable size. Second, we did observe chromosomal abnormalities in differentiating *Rtel*^{-/-} ES cells (Figure 6J) that indicate that genetic instability in those cells is not restricted to telomeres, consistent with recombination between telomeric DNA and intrachromosomal sequences (Figures 6J and 6K and legend). A role for RTEL in preventing illegitimate recombination is also compatible with the high level of RTEL expression in meiotic cells of the testis (Figure 2B). However, *Rtel*^{-/-} ES cells did not show deletions similar to those observed in *dog-1* mutant animals (see Supplemental Data for data and further discussion).

Rtel Is Required to Prevent Chromosomal Instability in Differentiating ES Cells

The very rapid onset of chromosomal instability in a minor subset of differentiating *Rtel*^{-/-} ES cells (Figure 5) is surprising. While chromosome fusions were most abundant after 48 hr, other types of abnormalities were already observed in a minority of cells 4 hr following induction of differentiation (Figure 5). What could be the immediate change(s) that trigger the chromosomal instability and demise of differentiating *Rtel*^{-/-} ES cells and embryos? It has been reported that DNA damage responses involving p53 are activated upon differentiation (Aladjem et al., 1998). However, we could not rescue the *Rtel*^{-/-} mutant phenotype by breeding with p53^{-/-} mice (data not shown). We assume that the genetic instability in differentiating *Rtel*^{-/-} ES is triggered by either posttranslational modifications of proteins or changes in gene expression. For example, a decrease in telomerase activity upon differentiation (Armstrong et al., 2000) could explain the increased number of fusions in differentiating *Rtel*^{-/-} ES cells (Figure 5L), as active

telomerase could be required to rescue critically short telomeres (Figure 7). Alternatively, telomerase in undifferentiated ES cells could “cap” the single-strand overhang present at telomeres and prevent their involvement in recombination reactions (Blackburn, 2000). Clearly, *Rtel*^{-/-} ES cells provide an excellent model for further studies of DNA damage responses and telomerase activity in relation to differentiation and genetic instability.

***Rtel* and the Differences in Telomere Length between Murine Species**

The chromosomal location of *Rtel* and its role in the elongation of telomeres in chromosomes derived from the *M. spretus* parent in F1 cells (Figure 6) are compatible with *Rtel* being the candidate gene(s) previously implicated in telomere length regulation (Zhu et al., 1998). Based on the observations reported here, we propose that RTEL, by preventing recombination between telomere repeats, is a primary determinant of telomere length in the mouse. How is *Rtel* related to the differences in telomere length between *M. spretus* and *M. musculus*? The RTEL protein sequence of both species is very similar, and no differences in overall expression pattern or promoter sequences have been identified. However, we did note differences in *Rtel* transcripts between the two species (Figure 1C). Whereas full-length *M. musculus Rtel* transcripts were readily obtained, full-length *M. spretus Rtel* transcripts were rare (Figure 1C). The predominant *M. spretus* transcript utilizes a secondary 3' splice site in exon 32, which results in the deletion of 18 nt. A possible explanation for this difference is a nucleotide divergence between the two *Mus* species at position -24 relative to exon 32. This nucleotide difference creates a new binding site for U2AF65, the large subunit of U2 snRNP auxiliary factor (Maniatis and Tasic, 2002; Kent et al., 2003) and, as a consequence, an alternative 3' splice site for exon 32 in *M. spretus* that does not exist in *M. musculus*. Differences resulting from alternative splicing of *Rtel* transcripts affect the carboxy terminus of the RTEL protein and create a novel CK1 phosphorylation site potentially disturbing the predicted functional interaction with PCNA. Further studies are needed to clarify if alternative splicing indeed provides an explanation for the apparent hypomorphic *M. spretus Rtel* allele and to delineate the precise difference in RTEL protein structure, expression, or posttranslational modification between the two species in relation to their widely different telomere lengths.

Role of RTEL at Telomeres

In addition to telomere length variation between different organisms, large variations in the telomere length at individual chromosome ends also exist in individual human and murine cells (Lansdorp et al., 1996; Martens et al., 2000; Zijlmans et al., 1997). For example, very short telomeres were also observed, be it at a low frequency, in *Rtel*^{+/+} ES cells (Figure 4E). Perhaps RTEL activity in wild-type cells increases the chance of (but does not guarantee) successful resolution of higher order structures of G-rich DNA. The limiting factor could be the chance of a functional interaction between RTEL and proliferating cell nuclear antigen (PCNA) via the PIP box motif in RTEL (Figure 1D). PCNA is involved in many

aspects of DNA replication and processing, and it has been proposed that sequential and regulated binding of PIP motif-containing proteins to PCNA may contribute to the ordering of events during DNA replication and repair (Warbrick, 2000). In *Saccharomyces cerevisiae*, the DNA helicase Rrm3p both interacts with PCNA via a PIP-box motif (Schmidt et al., 2002) and promotes replication fork progression through telomeric and subtelomeric DNA (Ivessa et al., 2002). Telomerase also interacts with PCNA and the lagging-strand DNA replication machinery in *S. pombe* (Dahlen et al., 2003) and, during macronuclear development but not in vegetatively growing cells, in the ciliate *Euplotes crassus* (Ray et al., 2002). Interactions of RTEL and telomerase with PCNA and other components of the replication and DNA repair machinery could be developmentally controlled in mammalian cells as well, perhaps explaining the increased genetic instability in *Rtel*^{-/-} ES cells upon differentiation. Presently, it is not clear if RTEL is part of the normal telomere replication machinery or is recruited to replication forks stalled at G4 DNA. While RTEL is localized in the nucleus (Figures 2C and 2E), the majority of RTEL foci did not show clear overlap with PCNA (Figures 2D and 2F-2H), and further studies are needed to distinguish between these possibilities.

Functional Relationship of *Rtel* to Other Telomere Maintenance Factors

Telomere length is regulated by highly dynamic and complex processes that are cell cycle-dependent and developmentally controlled (Zakian, 1996; McEachern et al., 2000; Ray et al., 2002). A surprisingly large number of helicases has been implicated in telomere homeostasis. In *S. cerevisiae*, at least four different helicases, including Pif1p, Rrm3p, Sgs1p, and Dna2p, have been reported to be involved in telomere function (Schulz and Zakian, 1994; Ivessa et al., 2002; Choe et al., 2002). In humans, members of the RecQ helicase family, including the Werner and Bloom syndrome helicases, are known to interact with telomeres (Schulz et al., 1996; Opresko et al., 2002; Hickson, 2003). Here, we demonstrate that RTEL is yet another helicase-like protein with an important role in telomere maintenance. It is possible that other helicases perform functions similar to RTEL. For example, in cells with insufficient expression of RTEL (or in cells that do not express the correct RTEL partners), the proposed function of RTEL could be executed by BRCA1 binding helicase-like protein BACH1 (Cantor et al., 2001) or by members of the RecQ helicase family (Hickson, 2003). Stochastic loss of telomeres has been reported in cells deficient in WRN protein (Schulz et al., 1996; Bai and Murnane, 2003), and the defective helicases associated with Werner and Bloom syndrome are known to be stimulated by interaction with the telomere binding protein TRF2 (Opresko et al., 2002) and are capable of unwinding telomeric G4 DNA (Mohaghegh et al., 2001). These proteins could also play a role in the resolution of higher order structures of telomeric DNA and thereby assist in the maintenance of telomere length and function. Future studies will no doubt reveal the role of RTEL relative to these other molecules in telomere function and the growth of normal and malignant cells.

Experimental Procedures

Isolation of *Rtel* Genomic DNA

Murine genomic DNA containing the *Rtel* gene was obtained from BAC RPCI-23-60M5 (CIHR Genome Resource Facility, Toronto, Canada), which was identified by hybridization with EST AA030845 (exons 22–34 of *Rtel*) as well as with cDNAs from the flanking genes *Stathm3* (AA058212) and *Arfrp1* (all from ATCC, Manassas, VA). For determination of the exon/intron structure, EcoRI or EcoRI/NcoI fragments, subcloned in pBluescript KS II+ (Stratagene), were isolated and hybridized with the full-length cDNA. Plasmids containing coding sequences were sequenced at the NAPS facility (University of British Columbia, Vancouver, Canada). To identify the transcription start site, 5' RACE was performed using Marathon-Ready cDNA from Balb/c testis (BD Biosciences Clontech, Palo Alto, CA). Five different start sites within a 65 bp region were found. The 5' UTR genomic sequence was generated by PCR on DNA isolated from Balb/c liver. Genomic DNA was isolated from skin fibroblasts of *M. spretus* (Jackson Laboratory, Bar Harbor, ME), and sequencing was done on amplified genomic DNA.

Cloning of *Rtel* cDNA

RNA was isolated from *M. spretus* and *M. musculus* (Balb/c) adult testis using Trizol (Invitrogen). First strand synthesis was done using oligo dT and Superscript II (Invitrogen). Full-length Balb/c and *M. spretus* cDNAs were assembled using the 5' primer with an EcoRI site inserted (AAGAATTCAGGCTGATATGCCAGGGTA), a 3' primer also with an EcoRI site (GAGAATTCCTTATTGCTTACTCGA), and internal forward (TGTGATTGTACAGGGCCTCCC) and reverse (CAATAGCCTGGTTCACAGCCC) primers.

Analysis of splice variants was done using the following primers: forward (exon 23) CGTGTTCCTCAAGATGCAG, reverse (exon 34) TTGCTTACTCCGATGAGGCTTC.

Generation of Mice Deficient for *Rtel*

The mouse *Rtel* genomic DNA fragments were cloned by PCR based on the mouse *Rtel* genomic sequence in the Celera database to build a target vector, which was designed to replace a 5 kb genomic fragment containing exons 7–9 with an SA-IRES- β geopA expression cassette. The targeting construct was linearized with NotI and electroporated into R1 ES cells and selected with G418 as described previously (Gertsenstein et al., 2002). Southern blot analysis was carried out to screen for the presence of a disrupted *Rtel* gene using BamHI (for the 5' external probe) and NsiI digestion (for the 3' external probe). We used two independently targeted ES cell clones to generate chimeric mice that subsequently were bred with 129S1 females to obtain germ-line transmission. The phenotypes of *Rtel*^{-/-} mutants derived from both targeted ES cell lines were indistinguishable.

Genotyping

PCR and Southern blot analysis were applied for genotyping. PCR was performed on ear-punched DNA. Primers to amplify the targeted allele were sense primer, located in intron 6 (TGTGTTTCTAGCCTCTGCAGCT) and antisense primer specific for the SA-IRES- β geopA cassette (GGGACAGGATAAGTATGACATCA). The primers to amplify the wild-type *Rtel* allele were sense primer locating on intron 7 (CCTTGAGGCTCTGTGTACAGA) and antisense primer locating on intron 8 (GACATCAGTAGCCATCAGCTT). Southern blot analysis was undertaken using standard protocols.

Northern Blot Analysis

Total RNA from flash-frozen mouse tissues was extracted using TRIzol (Life Technologies, Inc.), while total RNA from the cells was purified using the RNeasy Mini Kit (Qiagen). RNA (20 μ g of total) was fractionated on a 1% agarose-formaldehyde gel and transferred to Hybond nylon membrane (Amersham). Hybridization was carried out in ExpressHyb (Clontech) containing 2×10^6 cpm/ml probe.

Subcellular Expression of RTEL

Details of the experimental procedures used to study the expression and subcellular localization of epitope-tagged RTEL are described in Supplemental Data.

Derivation of *Rtel*^{-/-} ES Cells

Rtel^{+/-} mice (129S1 background) were intercrossed, and the day that vaginal plugs were detected was designated embryonic day 0.5 (E0.5). Blastocysts were flushed and then cultured in the ES culture medium to establish cell lines.

Culture and Cell Cycle Analysis of ES Cells

Rtel^{+/+}, *Rtel*^{+/-}, and *Rtel*^{-/-} ES cells were maintained under standard culture conditions in the presence of LIF on gelatin coated dishes, as described previously (Gertsenstein et al., 2002). For in vitro differentiation in semisolid medium, the cells were plated at 1500 cells per dish in methylcellulose medium (ES-Cult M3120, StemCell Technologies Inc., Vancouver, Canada). For differentiation in liquid culture, cells were plated in medium without LIF onto culture dishes that were not treated with gelatin. Cell cycle analysis was performed as described (Aladjem et al., 1998) with minor modifications. ES cells were grown with or without LIF for 30 min at 37°C in the presence of 30 μ M BrdU prior to fixation with ethanol and staining with propidium iodide and anti-BrdU-FITC antibody (Becton Dickinson, San Jose, CA) following the protocol supplied by Becton Dickinson. Flow cytometry data files were acquired on a FACSCalibur Flow Cytometer (Becton Dickinson), and data were analyzed using CellQuest and WinMDI software.

Telomere Length Analysis

The average telomere length in various cells was measured by flow FISH (Rufer et al., 1998) using modifications (including fixed bovine thymocytes as internal controls) as described (Baerlocher and Lansdorp, 2003). Q-FISH analysis was performed as previously described (Lansdorp et al., 1996; Zijlmans et al., 1997). Results of Q-FISH analysis are expressed in arbitrary units rather than telomere fluorescence units (TFU), because calibration based on hybridizations with plasmid DNA containing telomere inserts resulted in shorter average telomere values than were actually measured by flow FISH. Chromosomes from the *M. spretus* parent in cells derived from F1 animals obtained from crosses between a *M. musculus* (129S1 background) female and a *M. spretus* male were identified by including fluorescein labeled peptide nucleic acid (PNA) specific for repetitive DNA present at centromeres (FI-OO-CTTCGTTGGAAACGGGGT) at 0.3 μ g/ml together with Cy3-labeled (CCCTAA)_n PNA probe in the hybridization mixture. Analysis of terminal restriction fragments by Southern blot was performed as previously described (Harley et al., 1990).

Acknowledgments

We thank Gloria Shaw for help with cytogenetic procedures; Cam Smith for performing colony-forming assays; Susan McPhail and Peggy Olive for help with immunofluorescence procedures; Jacky Schein for analysis of BACs; Michael Schulzer for help with statistical analysis; Dixie Mager and Keith Humphries for helpful discussions; and Carolyn Price, Lea Harrington, and Peter Rowe for critically reading the manuscript. Peptide nucleic acid probes were generously provided by Applied Biosystems, Bedford, MA. This work is supported by the Terry Fox Foundation (P.M.L.); a CIHR grant to A.N.; and a Neuromuscular Disease Research Development Grant from the American Muscular Dystrophy Association (to H.D.). H.D. is the holder of CRC Chair. P.P.L.T. is a Senior Principal Research Fellow of the NHMRC of Australia. A.N. is a senior scientist of the CIHR.

Received: November 17, 2003

Revised: April 23, 2004

Accepted: April 28, 2004

Published: June 24, 2004

References

- Aladjem, M.I., Spike, B.T., Rodewald, L.W., Hope, T.J., Klemm, M., Jaenisch, R., and Wahl, G.M. (1998). ES cells do not activate p53-dependent stress responses and undergo p53-independent apoptosis in response to DNA damage. *Curr. Biol.* 8, 145–155.
- Armstrong, L., Lako, M., Lincoln, J., Cairns, P.M., and Hole, N. (2000).

- mTert expression correlates with telomerase activity during the differentiation of murine embryonic stem cells. *Mech. Dev.* 97, 109–116.
- Baerlocher, G.M., and Lansdorp, P.M. (2003). Telomere length measurements in leukocyte subsets by automated multicolor flow-FISH. *Cytometry* 55A, 1–6.
- Bai, Y., and Murmane, J.P. (2003). Telomere instability in a human tumor cell line expressing a dominant-negative WRN protein. *Hum. Genet.* 113, 337–347.
- Bai, C., Connolly, B., Metzker, M.L., Hilliard, C.A., Liu, X., Sandig, V., Soderman, A., Galloway, S.M., Liu, Q., Austin, C.P., and Caskey, C.T. (2000). Overexpression of M68/DcR3 in human gastrointestinal tract tumors independent of gene amplification and its location in a four-gene cluster. *Proc. Natl. Acad. Sci. USA* 97, 1230–1235.
- Blackburn, E.H. (2000). Telomere states and cell fates. *Nature* 408, 53–56.
- Blackburn, E.H. (2001). Switching and signaling at the telomere. *Cell* 106, 661–673.
- Blasco, M.A., Lee, H.-W., Hande, M.P., Samper, E., Lansdorp, P.M., DePinho, R.A., and Greider, C.W. (1997). Telomere shortening and tumor formation by mouse cells lacking telomerase RNA. *Cell* 91, 25–34.
- Cantor, S.B., Bell, D.W., Ganesan, S., Kass, E.M., Drapkin, R., Grossman, S., Wahrer, D.C., Sgroi, D.C., Lane, W.S., Haber, D.A., and Livingston, D.M. (2001). BACH1, a novel helicase-like protein, interacts directly with BRCA1 and contributes to its DNA repair function. *Cell* 105, 149–160.
- Cheung, I., Schertz, M., Rose, A., and Lansdorp, P.M. (2002). Disruption of *dog-1* in *Caenorhabditis elegans* triggers deletions upstream of guanine-rich DNA. *Nat. Genet.* 31, 405–409.
- Choe, W., Budd, M., Imamura, O., Hoopes, L., and Campbell, J.L. (2002). Dynamic localization of an Okazaki fragment processing protein suggests a novel role in telomere replication. *Mol. Cell. Biol.* 22, 4202–4217.
- Dahlen, M., Sunnerhagen, P., and Wang, T.S. (2003). Replication proteins influence the maintenance of telomere length and telomerase protein stability. *Mol. Cell. Biol.* 23, 3031–3042.
- de Lange, T. (2002). Protection of mammalian telomeres. *Oncogene* 21, 532–540.
- Gertsenstein, M., Lobe, C., and Nagy, A. (2002). ES cell-mediated conditional transgenesis. *Methods Mol. Biol.* 185, 285–307.
- Greider, C.W. (1996). Telomere length regulation. *Annu. Rev. Biochem.* 65, 337–365.
- Greider, C.W., and Blackburn, E.H. (1985). Identification of a specific telomere terminal transferase activity in *Tetrahymena* extracts. *Cell* 43, 405–413.
- Griffith, J.D., Comeau, L., Rosenfield, S., Stansel, R.M., Bianchi, A., Moss, H., and de Lange, T. (1999). Mammalian telomeres end in a large duplex loop. *Cell* 97, 503–514.
- Hackett, J.A., and Greider, C.W. (2003). End resection initiates genomic instability in the absence of telomerase. *Mol. Cell. Biol.* 23, 8450–8461.
- Harley, C.B., Futcher, A.B., and Greider, C.W. (1990). Telomeres shorten during ageing of human fibroblasts. *Nature* 345, 458–460.
- Hickson, I.D. (2003). RecQ helicases: caretakers of the genome. *Nat. Rev. Cancer* 3, 169–178.
- Ivessa, A.S., Zhou, J.Q., Schulz, V.P., Monson, E.K., and Zakian, V.A. (2002). *Saccharomyces Rrm3p*, a 5' to 3' DNA helicase that promotes replication fork progression through telomeric and subtelomeric DNA. *Genes Dev.* 16, 1383–1396.
- Kent, O.A., Reayi, A., Foong, L., Chilibeck, K.A., and MacMillan, A.M. (2003). Structuring of the 3' splice site by U2AF65. *J. Biol. Chem.* 278, 50572–50577.
- Kreepipuu, A., Blom, N., and Brunak, S. (1999). PhosphoBase, a database of phosphorylation sites: release 2.0. *Nucleic Acids Res.* 27, 237–239.
- Lansdorp, P.M., Verwoerd, N.P., van de Rijke, F.M., Dragowska, V., Little, M.-T., Dirks, R.W., Raap, A.K., and Tanke, H.J. (1996). Heterogeneity in telomere length of human chromosomes. *Hum. Mol. Genet.* 5, 685–691.
- Lustig, A.J. (2003). Clues to catastrophic telomere loss in mammals from yeast telomere rapid deletion. *Nat. Rev. Genet.* 4, 916–923.
- Makarov, V.L., Hirose, Y., and Langmore, J.P. (1997). Long G tails at both ends of human chromosomes suggest a C strand degradation mechanism for telomere shortening. *Cell* 88, 657–666.
- Maniatis, T., and Tasic, B. (2002). Alternative pre-mRNA splicing and proteome expansion in metazoans. *Nature* 418, 236–243.
- Marchler-Bauer, A., Anderson, J.B., DeWeese-Scott, C., Fedorova, N.D., Geer, L.Y., He, S., Hurwitz, D.I., Jackson, J.D., Jacobs, A.R., Lanczycki, C.J., et al. (2003). CDD: a curated Entrez database of conserved domain alignments. *Nucleic Acids Res.* 31, 383–387.
- Martens, U.M., Chavez, E.A., Poon, S.S., Schmoor, C., and Lansdorp, P.M. (2000). Accumulation of short telomeres in human fibroblasts prior to replicative senescence. *Exp. Cell Res.* 256, 291–299.
- McEachern, M.J., Krauskopf, A., and Blackburn, E.H. (2000). Telomeres and their control. *Annu. Rev. Genet.* 34, 331–358.
- McElligott, R., and Wellinger, R.J. (1997). The terminal DNA structure of mammalian chromosomes. *EMBO J.* 16, 3705–3714.
- Mieczkowski, P.A., Mieczkowska, J.O., Dominska, M., and Petes, T.D. (2003). Genetic regulation of telomere-telomere fusions in the yeast *Saccharomyces cerevisiae*. *Proc. Natl. Acad. Sci. USA* 100, 10854–10859.
- Mohaghegh, P., Karow, J.K., Brosh, J.R., Jr., Bohr, V.A., and Hickson, I.D. (2001). The Bloom's and Werner's syndrome proteins are DNA structure-specific helicases. *Nucleic Acids Res.* 29, 2843–2849.
- Moyzis, R.K., Buckingham, J.M., Cram, L.S., Dani, M., Deaven, L.L., Jones, M.D., Meyne, J., Ratliff, R.L., and Wu, J.-R. (1988). A highly conserved repetitive DNA sequence, (TTAGGG)_n, present at the telomeres of human chromosomes. *Proc. Natl. Acad. Sci. USA* 85, 6622–6626.
- Opresko, P.L., von Kobbe, C., Laine, J.P., Harrigan, J., Hickson, I.D., and Bohr, V.A. (2002). Telomere-binding protein TRF2 binds to and stimulates the Werner and Bloom syndrome helicases. *J. Biol. Chem.* 277, 41110–41119.
- Parkinson, G.N., Lee, M.P., and Neidle, S. (2002). Crystal structure of parallel quadruplexes from human telomeric DNA. *Nature* 417, 876–880.
- Petes, T.D., and Hill, C.W. (1988). Recombination between repeated genes in microorganisms. *Annu. Rev. Genet.* 22, 147–168.
- Ray, S., Karamysheva, Z., Wang, L., Shippen, D.E., and Price, C.M. (2002). Interactions between telomerase and primase physically link the telomere and chromosome replication machinery. *Mol. Cell. Biol.* 22, 5859–5868.
- Rufer, N., Dragowska, W., Thornbury, G., Roosnek, E., and Lansdorp, P.M. (1998). Telomere length dynamics in human lymphocyte subpopulations measured by flow cytometry. *Nat. Biotechnol.* 16, 743–747.
- Schmidt, K.H., Derry, K.L., and Kolodner, R.D. (2002). *Saccharomyces cerevisiae* RRM3, a 5' to 3' DNA helicase, physically interacts with proliferating cell nuclear antigen. *J. Biol. Chem.* 277, 45331–45337.
- Schulz, V.P., and Zakian, V.A. (1994). The *saccharomyces* PIF1 DNA helicase inhibits telomere elongation and de novo telomere formation. *Cell* 76, 145–155.
- Schulz, V.P., Zakian, V.A., Ogburn, C.E., McKay, J., Jarzabowicz, A.A., Edland, S.D., and Martin, G.M. (1996). Accelerated loss of telomeric repeats may not explain accelerated replicative decline of Werner syndrome cells. *Hum. Genet.* 97, 750–754.
- Sen, D., and Gilbert, W. (1988). Formation of parallel four-stranded complexes by guanine-rich motifs in DNA and its implications for meiosis. *Nature* 334, 364–366.
- Singer, M.S., and Gottschling, D.E. (1994). TLC1: template RNA component of *Saccharomyces cerevisiae* telomerase. *Science* 266, 404–409.
- Takai, H., Smogorzewska, A., and de Lange, T. (2003). DNA damage foci at dysfunctional telomeres. *Curr. Biol.* 13, 1549–1556.

- Vega, L.R., Mateyak, M.K., and Zakian, V.A. (2003). Getting to the end: telomerase access in yeast and humans. *Nat. Rev. Mol. Cell Biol.* 4, 948–959.
- von Zglinicki, T. (2002). Oxidative stress shortens telomeres. *Trends Biochem. Sci.* 27, 339–344.
- Warbrick, E. (2000). The puzzle of PCNA's many partners. *Bioessays* 22, 997–1006.
- Williamson, J.R., Raghuraman, M.K., and Cech, T.R. (1989). Monovalent cation-induced structure of telomeric DNA: the G-quartet model. *Cell* 59, 871–880.
- Zakian, V.A. (1995). Telomeres: beginning to understand the end. *Science* 270, 1601–1607.
- Zakian, V.A. (1996). Structure, function, and replication of *Saccharomyces cerevisiae* telomeres. *Annu. Rev. Genet.* 30, 141–172.
- Zhu, L., Hathcock, K.S., Hande, P., Lansdorp, P.M., Seldin, M.F., and Hodes, R.J. (1998). Telomere length regulation in mice is linked to a novel chromosome locus. *Proc. Natl. Acad. Sci. USA* 95, 8648–8653.
- Zhu, X.D., Niedernhofer, L., Kuster, B., Mann, M., Hoeijmakers, J.H., and de Lange, T. (2003). ERCC1/XPF removes the 3' overhang from uncapped telomeres and represses formation of telomeric DNA-containing double minute chromosomes. *Mol. Cell* 12, 1489–1498.
- Zijlmans, J.M., Martens, U.M., Poon, S.S., Raap, A.K., Tanke, H.J., Ward, R.K., and Lansdorp, P.M. (1997). Telomeres in the mouse have large inter-chromosomal variations in the number of T₂AG₃ repeats. *Proc. Natl. Acad. Sci. USA* 94, 7423–7428.

Accession Numbers

The GenBank accession numbers for *Rtel* full-length, promoter, and splice variant sequences (see Figure 1C) are the following: *M. musculus*, AY481619, AY48618, AY481620, AY481621, AY481622, AY481623, and AY481624; and *M. spretus*, AY530632, AY48612, AY481613, AY481614, AY481615, AY481616, and AY481617.